Supporting information of

Title:

A CuMg-MOF-74 derived stable Cu/MgO@SiO_2 for the hydrogenation of bis(2-hydroxyethyl) cyclohexane-1,4-dicarboxylate

Authors:

Zhili Chang [a], Guangquan Li [a], Xuemei Mu [a], Weitao Ou [b,*], Haolan Liu [c,*], Guangcheng Zhang [d,*]

[a] Lanzhou Petrochemical Research Center, Petrochemical Research Institute, PetroChina, Lanzhou 730060, China.

[b] Key Laboratory of Biomass Chemical Engineering of Ministry of Education, Department of Chemistry, Zhejiang University, Hangzhou 310028, China.

[c] Material Research Institute, Henan Academy of Sciences, Zhengzhou 450002, China.

[d] Zhejiang Hengyi Petrochemical Research Institute Co., Ltd., Hangzhou 311200, China.

* Corresponding author

Guangcheng Zhang & Haolan Liu & Weitao Ou

Email: ZhangGChem@163.com (G. Zhang) & haolan0128@163.com (H. Liu) & 847901057@qq.com (W. Ou)

Materials

Copper nitrate trihydrate ($Cu(NO_3)_2 \cdot 3H_2O$), magnesium nitrate hexahydrate ($Mg(NO_3)_2 \cdot 6H_2O$), *N*,*N*'-dimethylformamide (DMF), methanol (CH_3OH), ethanol (C_2H_5OH), and 1,4-dioxane were purchased from Sinopharm Chemical Reagent Co., Ltd. (Shanghai, China). Tetraethyl orthosilicate (TEOS), dimethyl 1,4-cyclohexanedicarboxylate (DMCD), and 1,4-cyclohexanedimethanol (CHDM) were bought from Aladdin Reagent Co., Ltd. (Shanghai, China). 2,5-Dihydroxyterephthalic acid (DHTA) was obtained from Macklin Biochemical Co., Ltd. (Shanghai, China). Bis(2-hydroxyethyl) cyclohexane-1,4-dicarboxylate (BHCD) was supplied from Hengyi Petrochemical Research Institute Co., Ltd. (Hangzhou, China). Deionized water (H_2O) was purchased from Wahaha Group Co., Ltd. (Hangzhou, China). All these chemicals were analytically pure and used directly without further purification.

***Preparation of reference* Cu/MgO**

At first, CuMg-DHTA was calcined at 400 °C for 4 h under air flow (60 $mL \cdot min^{-1}$) to obtain CuO-MgO. After that, CuO-MgO was pressed into granular (40–60 mesh), and then reduced at 300 °C under H_2 flow (60 $mL \cdot min^{-1}$) for 1 h to get Cu/MgO.

***Preparation of* MgO@SiO_2, Cu@SiO_2 *and* metallic Cu**

MgO@SiO_2 and Cu@SiO_2 were prepared the same as Cu/MgO@SiO_2, but only $Mg(NO_3)_2 \cdot 6H_2O$ was added in Mg-MOF-74 precursor for MgO@SiO_2, and only $Cu(NO_3)_2 \cdot 3H_2O$ was added in Cu-MOF-74 precursor for Cu@SiO_2.

Metallic Cu was synthesized via direct calcination of $Cu(NO_3)_2 \cdot 3H_2O$ at 400 °C under air flow (60 $mL \cdot min^{-1}$) for 4 h, followed by the reduction at 300 °C under H_2 flow (60 $mL \cdot min^{-1}$) for 1 h.

***Preparation of* Cu *catalysts supported by* MgO *with* SiO_2**

Cu/MgO-SiO_2-*WK* was synthesized *via* wet kneading (WK) method. Firstly, $Mg(OH)_2$ was prepared by the addition of $Mg(NO_3)_2 \cdot 6H_2O$ and aqueous ammonia

solution, while SiO_2 was prepared by the addition of TEOS at ethanol-ammonia solution. After that, 2.356 g $Mg(OH)_2$ and 1.992 g SiO_2 were stirred together in deionized water and calcined at 400 °C for 4 h under air flow (60 mL·min^{-1}) to obtain MgO-SiO_2. Next, 5.601 g $Cu(NO_3)_2 \cdot 3H_2O$ was dissolved in 20 mL deionized water with dispersed 4.000 g MgO-SiO_2. The mixture was stirred for 6 h, and dried at 80 °C in vacuum for 12 h. Finally, the solid was calcined at 400 °C for 4 h under air flow (60 mL·min^{-1}), then reduced at 300 °C under H_2 flow (60 mL·min^{-1}) for 1 h to get Cu/MgO-SiO_2-*WK* after being pressed into granular (40–60 mesh).

CuO/MgO/SiO_2-*IWI* was synthesized *via* incipient wetness impregnation (IWI) method. Typically, $Cu(NO_3)_2 \cdot 3H_2O$ was impregnated on $Mg(OH)_2$, and then kneaded together with SiO_2 achieved upon a precipitation procedure. After being dried, the solid was calcined and reduced to obtain CuO/MgO/SiO_2-*IWI*. On the other hand, CuO/SiO_2/MgO-*IWI* was prepared in the similar manner except that $Cu(NO_3)_2 \cdot 3H_2O$ was impregnated on SiO_2, and then kneaded together with $Mg(OH)_2$.

Cu/MgO/SiO_2-*CP* was synthesized *via* co-precipitation (CP) method. At first, $Cu(NO_3)_2 \cdot 3H_2O$ and $Mg(NO_3)_2 \cdot 6H_2O$ were added into NaOH solution. Next, the obtained $Cu(OH)_2$ and $Mg(OH)_2$ kneaded with SiO_2. After being dried, the solid was calcined and reduced to obtain Cu/MgO/SiO_2-*CP*.

Characterization

Powder X-ray diffraction (XRD) patterns were acquired using Cu *Kα* radiation ($\lambda = 0.15406$ nm) operating at 100 kV and 180 mA with a step of 0.02° and 5°·min^{-1} from 5 to 80° on a Rigaku SmartLab diffractometer. Inductively coupled plasma atomic emission spectroscopy (ICP-AES) was used to detect the element content on a Plasma-Spec-II spectrometer. Fourier transform infrared spectroscopy (FTIR) was collected in the wavenumber range of 4000–400 cm^{-1} using a Nicolet Is10 FTIR spectrometer. N_2 adsorption-desorption measurement was measured at –196 °C using an iPore 400 analyzer (Physichem Instruments Limited, China) after degasification at 100 °C in vacuum for 4 h. Thermogravimetric and differential thermal analysis (TG-DTA) was performed on a Netzsch STA 409 thermobalance

under a ramping rate of 10 °C·min^{-1} from 25 to 800 °C in air flow (30 mL·min^{-1}). Scanning electron microscopy (SEM) images were observed on a Hitachi SU8000 field emission scanning electron microscope, and the samples were coated with platinum to avoid charging. Transmission electron microscopy (TEM) images were obtained on a JEOL-2020AF microscope with an accelerating voltage of 200 kV. Before the test, the samples were dispersed in ethanol and grinded for 1 h in a mortar. After dilution in ethanol and further ultrasonic treatment, several drops of the suspension were dispersed on a molybdenum grid for TEM analysis. Map-scanning and line-scanning elemental energy dispersive spectroscopy (EDS) was carried out *via* a FEI TECNAI F30 microscope at 300 kV.

In-situ X-ray photoelectron spectroscopy (*in-situ* XPS) with Auger electron spectroscopy was conducted with a Thermo-Fischer ESCALAB 250Xi spectrometer. A monochromatic Al *Kα* (1486.6 eV) radiation source was applied and C 1*s* with the binding energy of 284.8 eV was used for calibration. Firstly, XPS measurement of C 1*s*, Cu 2*p* and Cu LMM binding energies for calcined samples was conducted at room temperature. To investigate the Cu chemical state, the sample was compressed into a thin disk and reduced in H_2/Ar (V/V = 1/9) flow (30 mL·min^{-1}) flow at 300 °C for 1 h in a reaction chamber. Afterwards, the sample was carefully transferred into the XPS measurement chamber under high vacuum conditions. Finally, XPS measurement was repeated for reduced catalyst.

H_2 temperature-programmed reduction (H_2-TPR) was carried out in the following procedures. 0.05 g calcined sample (40–60 mesh) was pretreated at 400 °C for 1 h in N_2 flow (30 mL·min^{-1}), and then cooled to 50 °C. Next, H_2/Ar (V/V = 1/9) flow (30 mL·min^{-1}) was shifted to the reactor, and the sample was heated to 400 °C with a ramping of 10 °C·min^{-1}. The online quadrupole mass spectrometer (OmniStarTM, GSD301, Switzerland) was used to monitor H_2 in effluent, and the consumption of H_2 was denoted as ***X***. After that, the sample was cooled to 50 °C under N_2 flow (30 mL·min^{-1}). And then, N_2O flow (30 mL·min^{-1}) was introduced into the sample. Following this, the reactor was purged with N_2 flow (30 mL·min^{-1}) to remove N_2O. Finally, H_2-TPR procedure was repeated, and the consumption of H_2

was denoted as ***Y***. The dispersion of Cu was calculated as follows.

$$CuO + H_2 \rightarrow Cu + H_2O, \text{ consumption of } H_2 = \boldsymbol{X} \quad \text{(S1)}$$

$$2Cu + N_2O \rightarrow Cu_2O + N_2 \quad \text{(S2)}$$

$$Cu_2O + H_2 \rightarrow 2Cu + H_2O, \text{ consumption of } H_2 = \boldsymbol{Y} \quad \text{(S3)}$$

$$\text{dispersion of Cu} = \frac{2 \times \text{moles of consumption of } H_2(\boldsymbol{Y})}{\text{moles of consumption of } H_2(\boldsymbol{X})} \times 100\% \quad \text{(S4)}$$

CO_2 temperature-programmed desorption (CO_2-TPD) was carried out in the following procedures. 0.05 g sample (40–60 mesh) was pretreated at 600 °C for 1 h in N_2 flow (30 mL·min^{-1}). After that, the sample was cooled to 50 °C and exposed to CO_2 flow (30 mL·min^{-1}) for 30 min. Finally, temperature-programmed desorption was conducted with a ramping of 10 °C·min^{-1} from 50 to 600 °C. CO_2 in effluent was measured on the online quadrupole mass spectrometer (OmniStarTM, GSD301, Switzerland), which was detected and recorded as a function of temperature. H_2 temperature-programmed desorption (H_2-TPD) was performed in the same process as above except that the sample was exposed to H_2 for 30 min, and temperature-programmed desorption was conducted from 50 to 350 °C.

Diffuse reflectance infrared Fourier transform spectroscopy (DRIFTS) measurement was performed on a Thermo Scientific Nicolet IS50 FTIR Spectrometer with a Praying Mantis high temperature reaction chamber. Firstly, 0.025 g tableted sample was put into the reaction chamber and then reduced at 300 °C (10 °C·min^{-1}) for 1 h under H_2 flow (30 mL·min^{-1}). After that, the sample was purged with N_2 flow (30 mL·min^{-1}) and cooled to 50 °C, and the background spectrum under this condition was recorded. Then, pure CO flow (30 mL·min^{-1}) was introduced into the reaction chamber. After adsorption, N_2 flow (30 mL·min^{-1}) was used to purge the CO gas. DRIFTS spectra were constantly taken during the purging procedure up till the peak remained unaltered.

Adsorption test of BHCD was carried out in the following procedures. Firstly, 1.0 g reduced catalyst and 0.1 g BHCD were dispersed in 10 mL 1,4-dioxane. Then, the supernatant was taken every 30 min and analyzed using a gas chromatograph

(Shimadzu, 14B) equipped with a 30 m capillary column (HP-5MS, USA) and a flame ionization detector.

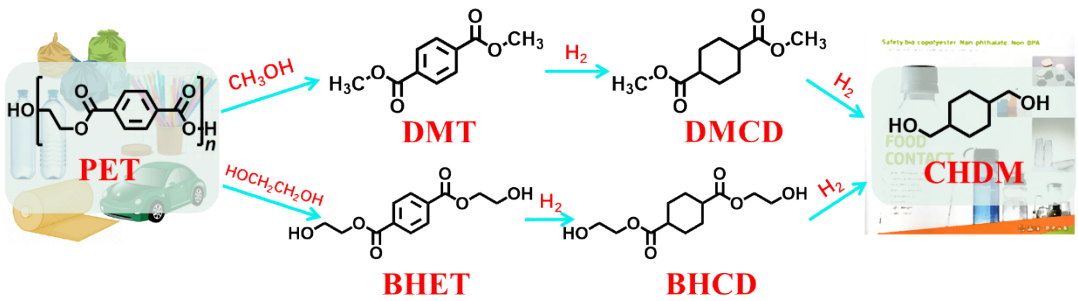

Scheme S1. Proposed reaction routes from PET to CHDM.

Table S1. Performance of Cu catalysts for the hydrogenation of DMCD to CHDM in fixed bed.

Catalyst	Temp. (°C)	Press. (MPa)	WHSV (h^{-1})	ω (wt%)	$n(H_2)/n$(DMCD) ($mol \cdot mol^{-1}$)	Con. (%)	Sel. (%)
$Cu/ZnO/ZrO_2$ [a]	220	8	0.44	10	467	99.4	97.4
$Cu/MgO/Al_2O_3$ [b]	220	6	0.09	10	403	100	99.8
$Cu/ZnO/Al_2O_3$ [c]	220	8	0.44	10	406	99.8	95.8
Cu/MgO [d]	220	6	1.2	20	220	98.7	98.2
Cu-CSNTs [e]	220	5	0.08	5	260	100	96.3
$Cu/Al\text{-}ZrO_2$ [f]	220	8	0.4	14	203	98.8	95.8
$Cu/MnO/Al_2O_3$ [g]	250	5	0.95	5	300	100	98.0
$Cu_1/Mg_3Sc_2O_6$ [h]	250	2	0.49	13	120	99.3	97.0

Reaction conditions: [a] 3.0 g cat., Cu content of 40.0wt%, solvent of methanol [1].

[b] 3.0 g cat., Cu content of 40.3wt%, solvent of methanol [2].

[c] 3.0 g cat., Cu content of 32.0wt%, solvent of methanol [3].

[d] 2.0 g cat., Cu content of 70.9wt%, solvent of methanol [4].

[e] 0.1 g cat., Cu content of 29.2wt%, solvent of methanol [5].

[f] 3.0 g cat., Cu content of 16.8wt%, solvent of methanol [6].

[g] 1.0 g cat., Cu content of 49.7wt%, solvent of methanol [7].

[h] 1.0 g cat., Cu content of 19.2wt%, solvent of 1,4-dioxane [8].

Table S2. Performance of Cu catalysts for the hydrogenation of BHCD to CHDM in fixed bed.

Catalyst	Temp. (°C)	Press. (MPa)	WHSV (h^{-1})	ω (wt%)	$n(H_2)/n$(BHCD) ($mol \cdot mol^{-1}$)	Con. (%)	Sel. (%)
$Cu/MgAl_2O_4$ [a]	240	4	0.525	20	377	99.1	96.5
$Cu/MgO@SiO_2$ [b]	**260**	**2.5**	**0.8**	**20**	**155**	**99.2**	**97.1**

Reaction conditions: [a] 0.8 g cat., Cu content of 33.0wt%, solvent of 1,4-dioxane [9].

[b] 1.0 g cat., Cu content of 36.8wt%, solvent of 1,4-dioxane (This work).

Table S3. The properties of CuMg-DHTA and CuMg-DHTA@SiO_2.

Sample	Lattice parameter [a] (***a***=***b***, ***c***, nm)	S_{BET} [b] ($m^2 \cdot g^{-1}$)	V_{pore} [c] ($cm^3 \cdot g^{-1}$)
CuMg-DHTA	2.5987, 0.6252	961	0.57
CuMg-DHTA@SiO_2	2.5979, 0.6246	537	0.29
Mg-MOF-74	2.5997, 0.6259	–	–

[a] Calculated using Bragg Equation from the result of XRD.

[b] Calculated by Brunauer-Emmett-Teller (BET) method.

[c] Measured by Barrett-Joyner-Halenda (BJH) method.

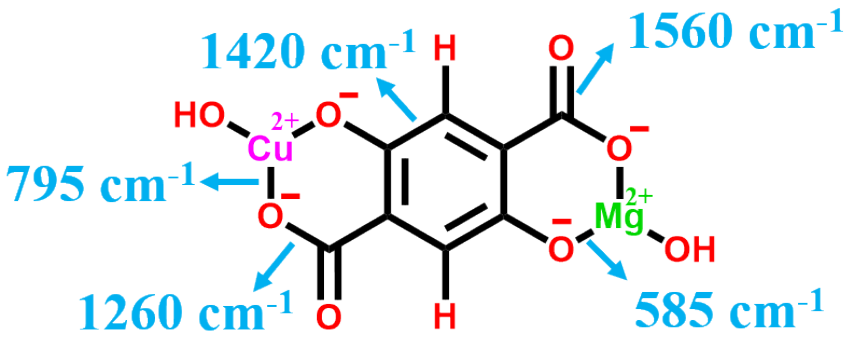

Scheme S2. The framework structure of CuMg-DHTA.

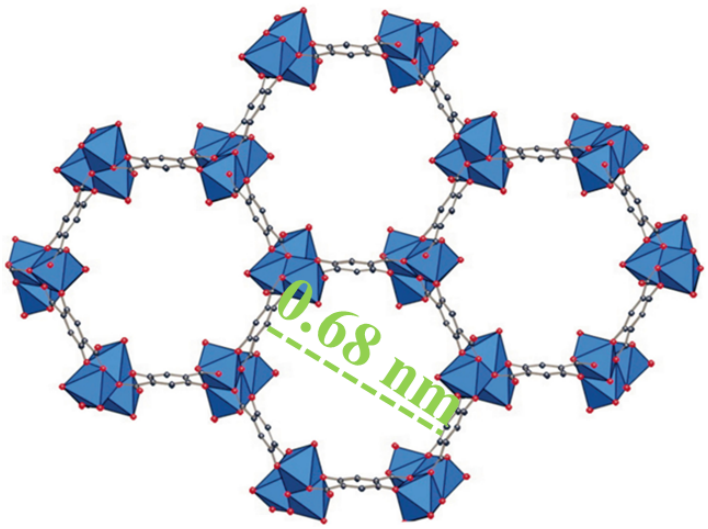

Scheme S3. Channel diagram of CuMg-DHTA.

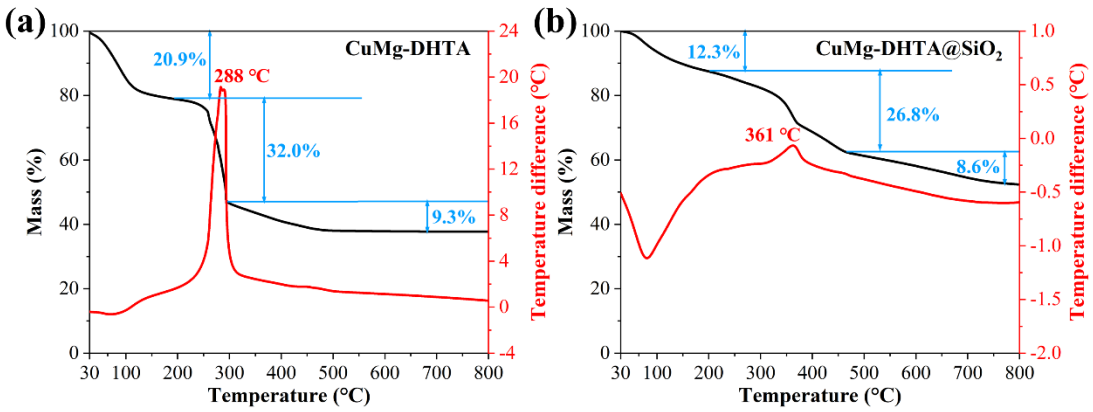

Fig. S1. Thermal analysis of CuMg-DHTA (a) and CuMg-DHTA@SiO_2 (b) under air flow.

(1) According to Fig. S1a, the remaining mass ratio of CuMg-DHTA was 100% – 20.9% = 79.1%, and the rest of mass ratio of CuO-MgO was 79.1% – 32.0% – 9.3% = 37.8%.

(2) Based on Fig. S1b, the remaining mass ratio of CuMg-DHTA@SiO_2 was 100% – 12.3% = 87.7%, and the rest of mass ratio of CuO-MgO@SiO_2 was 87.7% – 26.8% – 8.6% = 52.3%.

(3) The mass ratio of introduced SiO_2 (donated ω) was calculated by the equation of 79.1% / 37.8% = (87.7% – ω) / (52.3% – ω), and the calculated ω was 19.9%. So, the weight percentage of SiO_2 in CuMg-DHTA@SiO_2 was 19.9% / 87.7% = ***22.7%***.

Table S4. Textural properties of CuO-MgO and CuO-MgO@SiO_2.

Catalyst	S_{BET} [a] ($m^2 \cdot g^{-1}$)	V_{pore} [b] ($cm^3 \cdot g^{-1}$)
CuO-MgO	24	0.18
CuO-MgO@SiO_2	146	0.75

[a] Calculated by Brunauer-Emmett-Teller (BET) method.

[b] Simulated by quenched solid density functional theory (QSDFT) method.

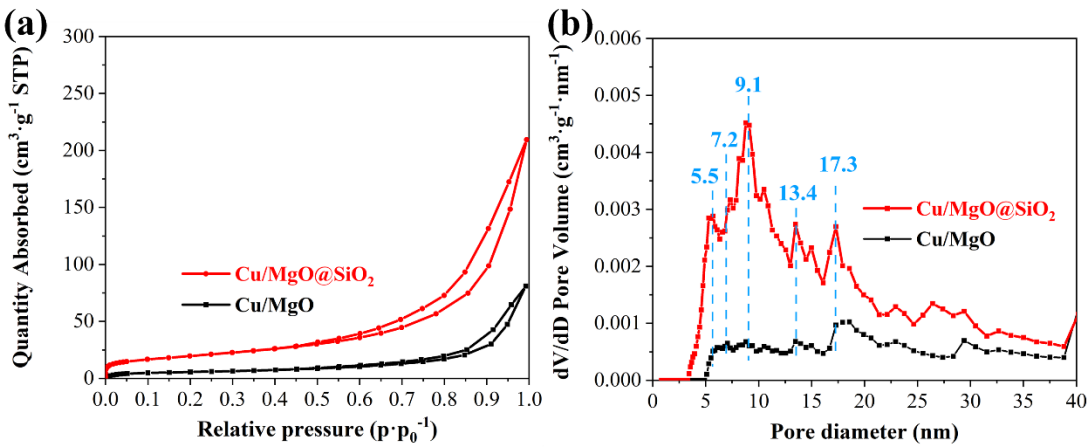

Fig. S2. N_2 adsorption-desorption isotherms (a) and pore size distributions (b) of Cu/MgO and Cu/MgO@SiO_2.

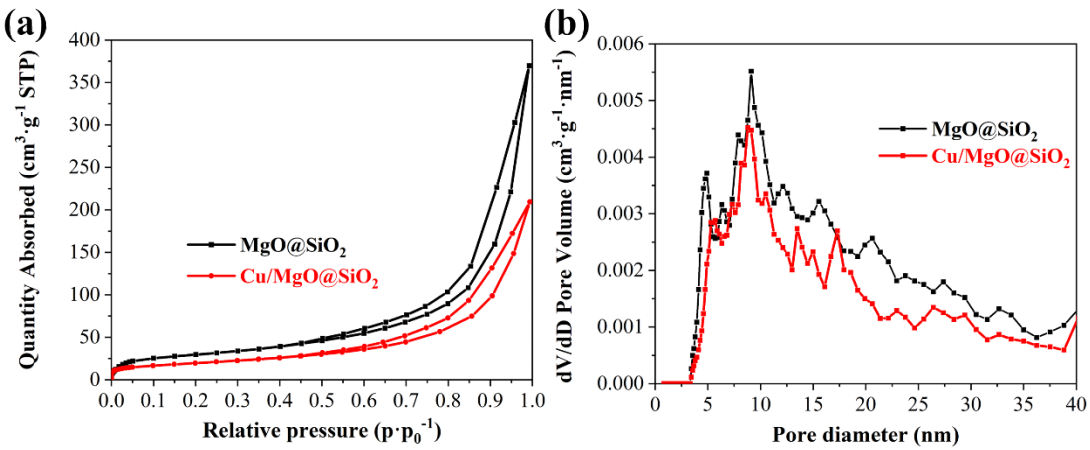

Fig. S3. N_2 adsorption-desorption isotherms (a) and pore size distributions (b) of MgO@SiO_2 and Cu/MgO@SiO_2.

Table S5. Textural properties of MgO@SiO_2 and Cu/MgO@SiO_2.

Sample	S_{BET} [a] ($m^2 \cdot g^{-1}$)	V_{pore} [b] ($cm^3 \cdot g^{-1}$)
MgO@SiO_2	137	0.71
Cu/MgO@SiO_2	104	0.52

[a] Calculated by Brunauer-Emmett-Teller (BET) method.

[b] Simulated by quenched solid density functional theory (QSDFT) method.

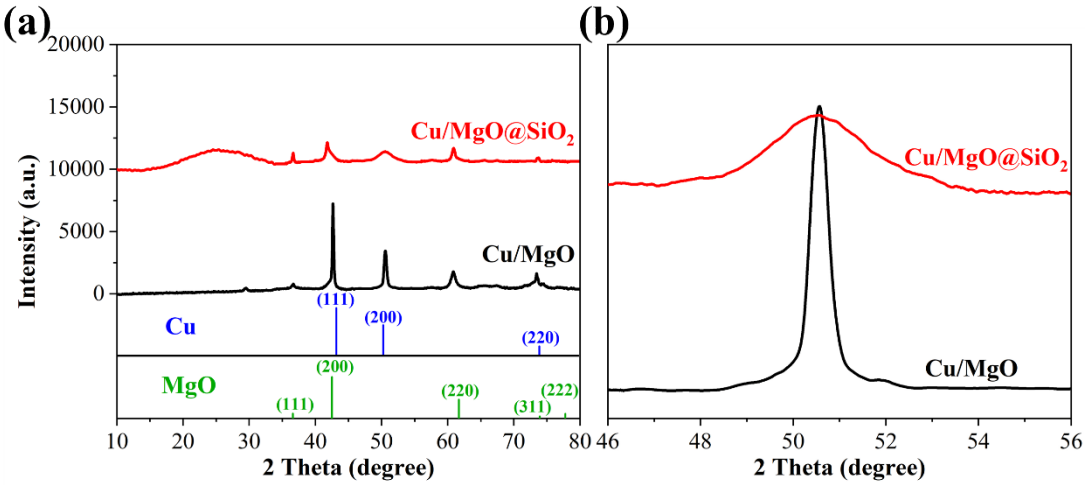

Fig. S4. XRD patterns (a) and enlarged diffraction at 46–56° (b) of Cu/MgO and Cu/MgO@SiO_2.

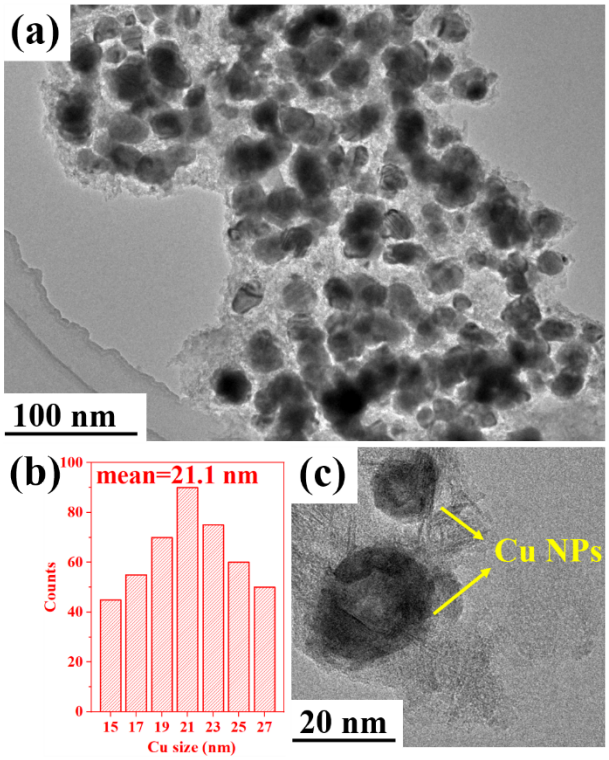

Fig. S5. TEM images (a, c) and distributions of Cu NPs (b) of Cu/MgO.

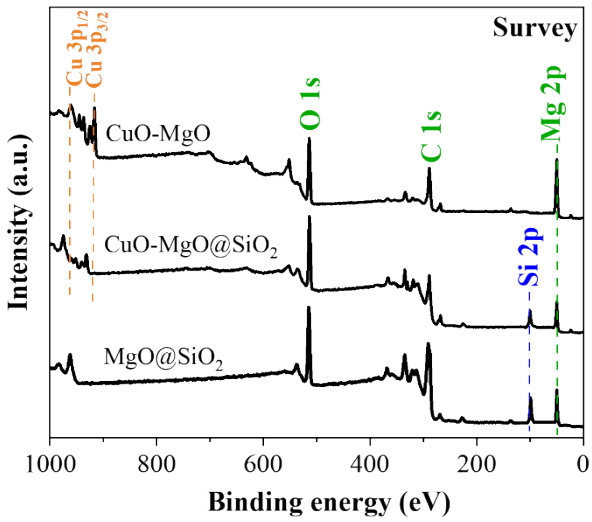

Fig. S6. XPS of survey in CuO-MgO, CuO-MgO@SiO_2 and MgO@SiO_2.

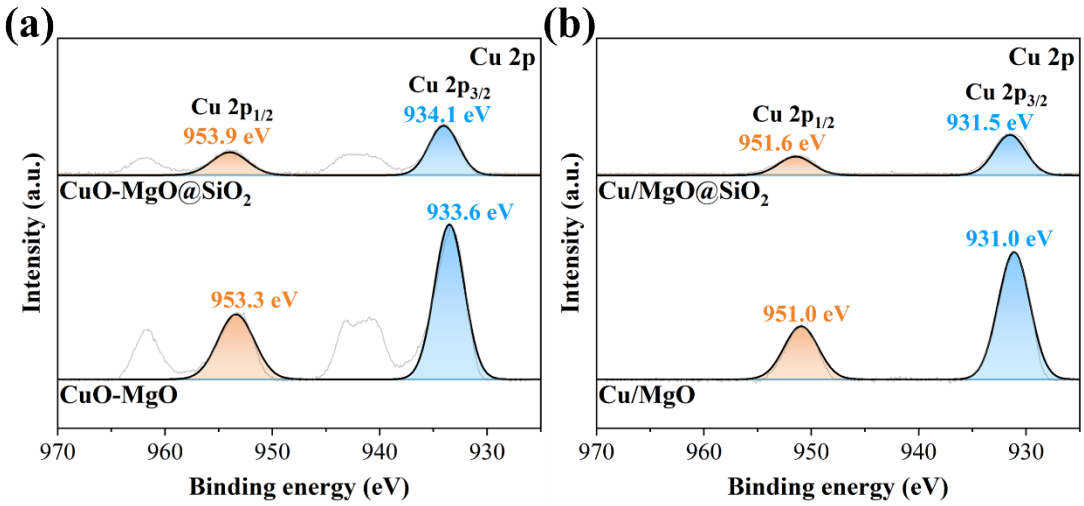

Fig. S7. Binding energy of Cu 2*p* in CuO-MgO and CuO-MgO@SiO_2 (a), Cu/MgO and Cu/MgO@SiO_2 (b).

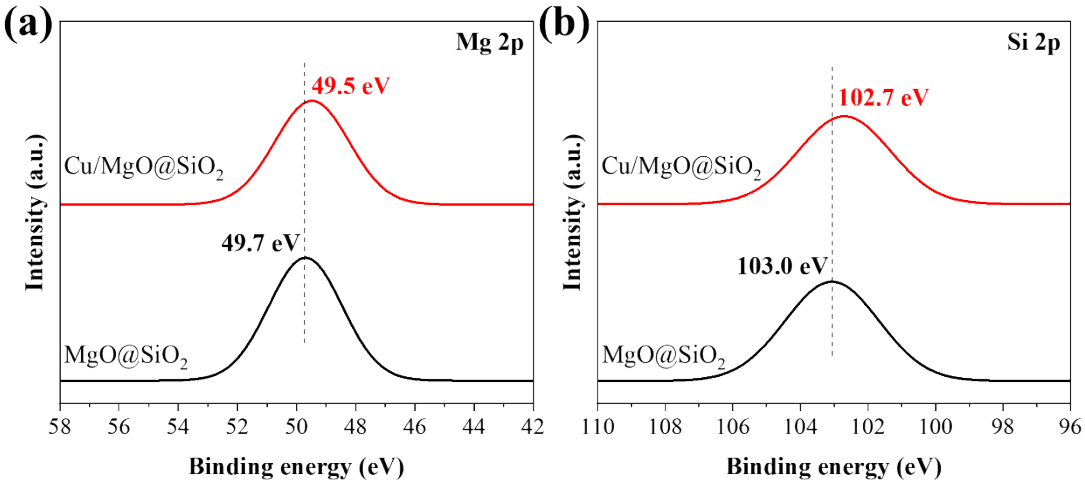

Fig. S8. Binding energies of Mg 2*p* (a) and Si 2*p* (b) in $MgO@SiO_2$ and $Cu/MgO@SiO_2$.

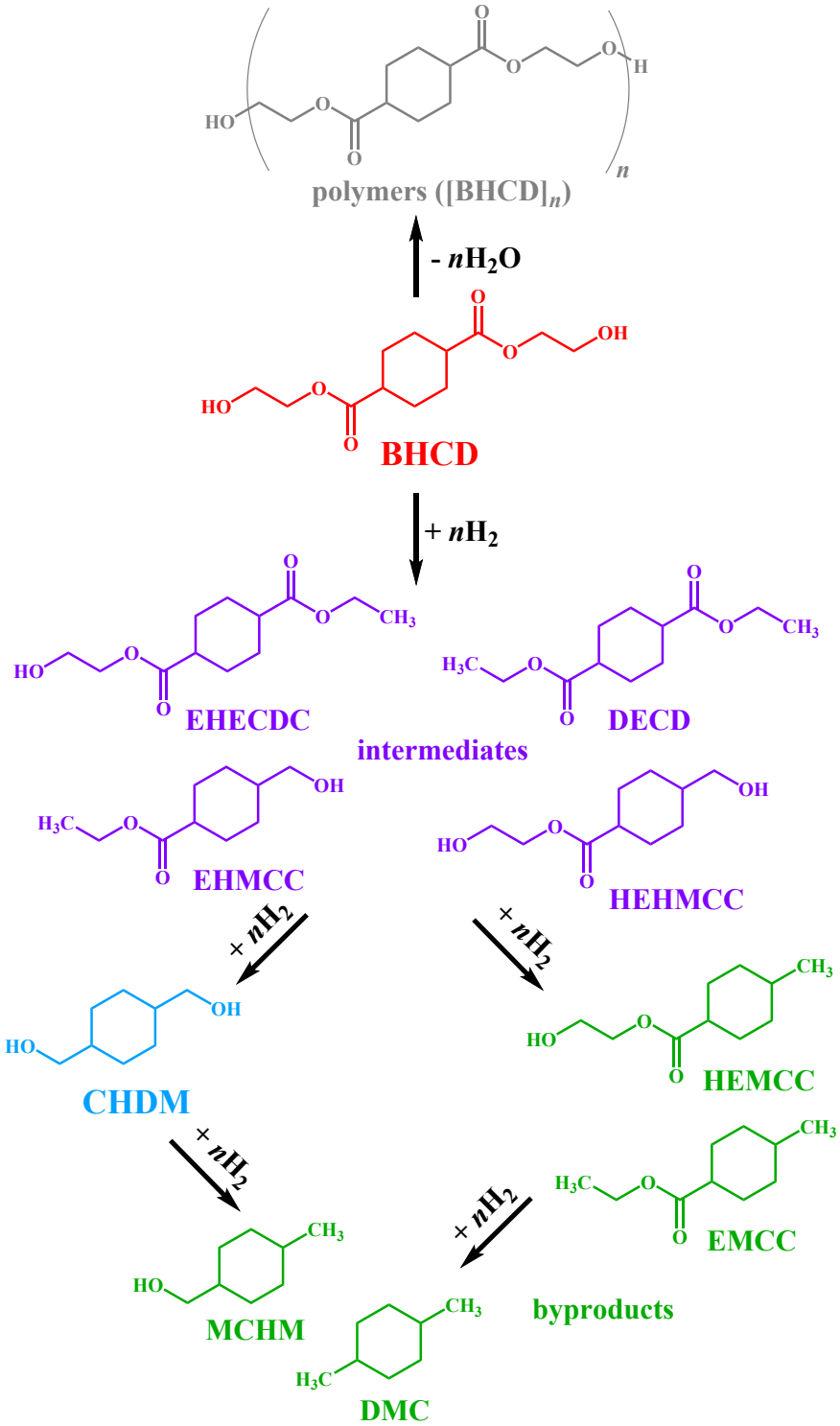

Scheme S4. Reaction pathway for the hydrogenation of BHCD to CHDM.

The reaction pathway for the hydrogenation of BHCD to CHDM was checked *via* gas chromatography-electron ionization mass spectrometry (GC-EI-MS, Agilent 7250 GC/Q-TOF).

Table S6. The hydrogenation of BHCD to CHDM over different Cu catalysts.

Entry	Catalyst	Conversion (%)	Selectivity (%)			
		BHCD	polymers	intermediates	CHDM	byproducts
1 [a]	Cu/MgO@SiO_2	99.2	0.8	0.8	97.1	1.3
2 [a]	MgO@SiO_2	7.5	99.2	0.4	0.3	0.1
3 [a]	Cu/MgO	49.8	1.9	8.7	82.3	7.1
4 [a]	Cu@SiO_2	33.1	10.4	16.5	65.8	7.3
5 [b]	metallic Cu	14.3	4.5	26.3	56.5	12.7

Reaction conditions: [a] 1 g cat., 260 °C, 2.5 MPa H_2, WHSV=0.8 h^{-1}, $n(H_2)/n(BHCD)$=155 mol·mol^{-1}.
[b] 0.368 g cat., 260 °C, 2.5 MPa H_2, WHSV=0.8 h^{-1}, $n(H_2)/n(BHCD)$=155 mol·mol^{-1}.

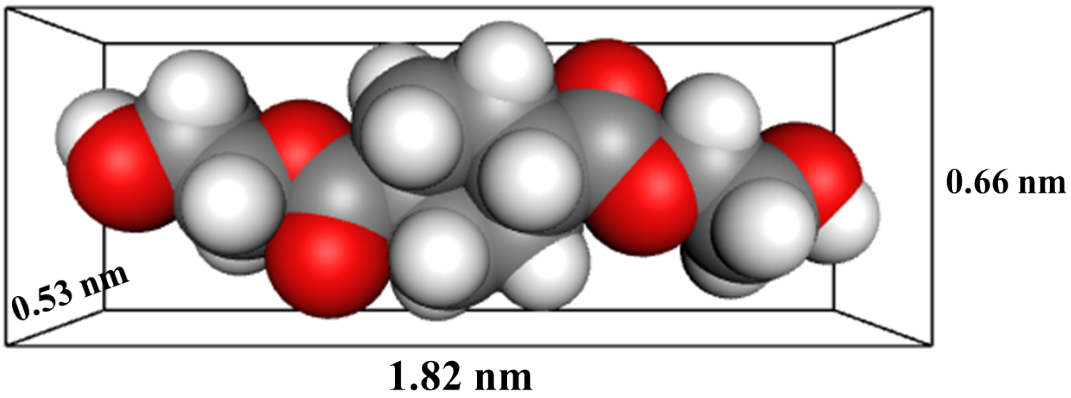

Fig. S9. Size of bis(2-hydroxyethyl) cyclohexane-1,4-dicarboxylate (BHCD).

The size of BHCD is 1.82 nm × 0.53 nm × 0.66 nm. **Copyright from** https://jerkwin.github.io/2016/06/24/%E5%88%86%E5%AD%90%E5%B0%BA%E5%AF%B8%E5%A4%A7%E5%B0%8F%E7%9A%84%E8%AE%A1%E7%AE%97/

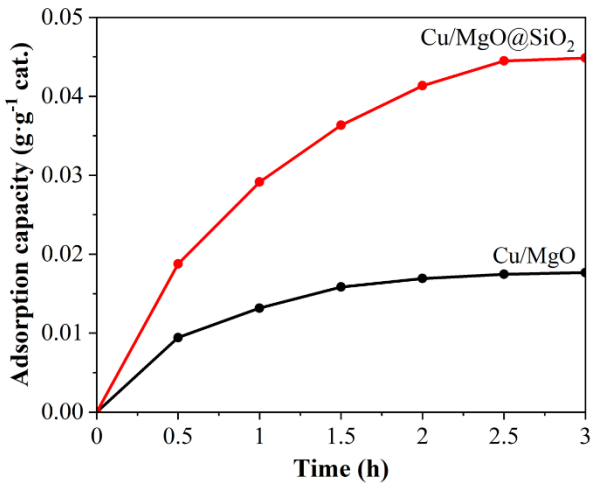

Fig. S10. The adsorption capacity of BHCD over Cu/MgO and Cu/MgO@SiO_2.

Adsorption conditions: 1 g cat., 0.1 g BHCD, 10 mL 1,4-dioxane, 25 °C, 101.325 kPa.

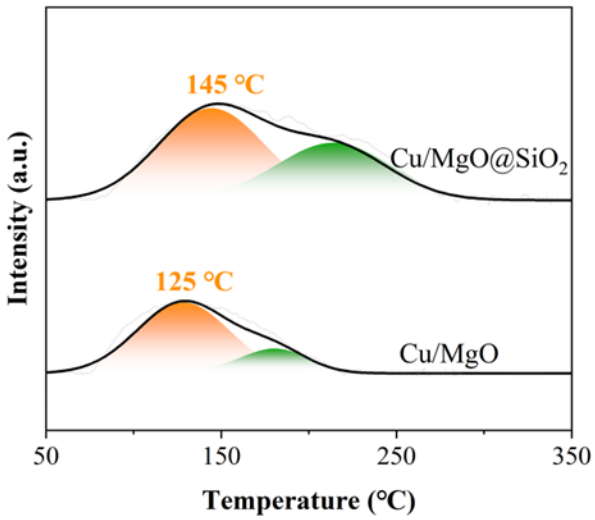

Fig. S11. H_2-TPD profiles of Cu/MgO and Cu/MgO@SiO_2.

Table S7. The properties of different Cu catalysts.

Catalyst	Cu size [a] (nm)	Cu content [b] (%)	Cu dispersion [c] (%)	S_{BET} [d] ($m^2 \cdot g^{-1}$)	V_{pore} [e] ($cm^3 \cdot g^{-1}$)	Basicity [f] ($\mu mol \cdot g^{-1}$)
Cu/MgO@SiO_2	**4.6**	**36.8**	**22.6**	**104**	**0.52**	**480**
Cu/MgO-SiO_2-*WK*	7.9	36.6	13.1	77	0.40	340
Cu/MgO/SiO_2-*IWI*	11.3	36.3	9.3	51	0.28	270
Cu/SiO_2/MgO-*IWI*	15.2	37.0	6.9	44	0.25	250
Cu/MgO/SiO_2-*CP*	13.8	37.2	7.5	48	0.26	240

[a] Calculated using Debye-Scherrer Formula from the result of XRD.

[b] Determined using ICP-AES.

[c] Calculated according to the result of N_2O titration.

[d] Calculated by Brunauer-Emmett-Teller (BET) method.

[e] Measured by Barrett-Joyner-Halenda (BJH) method.

[f] Calculated from the result of CO_2-TPD.

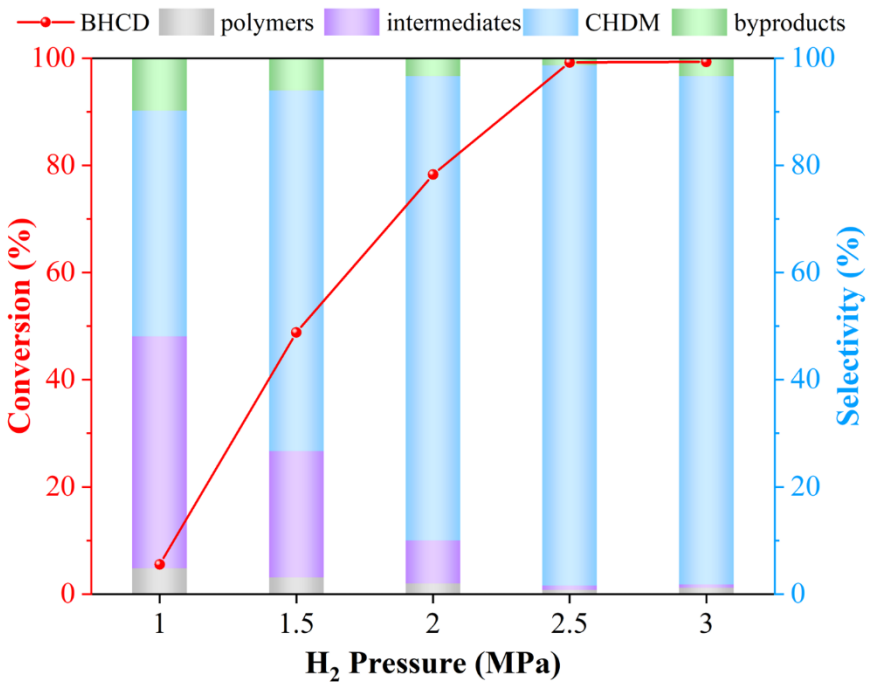

Fig. S12. Performance of Cu/MgO@SiO_2 under varied H_2 pressures.

Reaction conditions: 1 g cat., ω=20wt%, 260 °C, WHSV=0.8 h^{-1}, $n(H_2)/n(BHCD)$=155 mol·mol^{-1}.

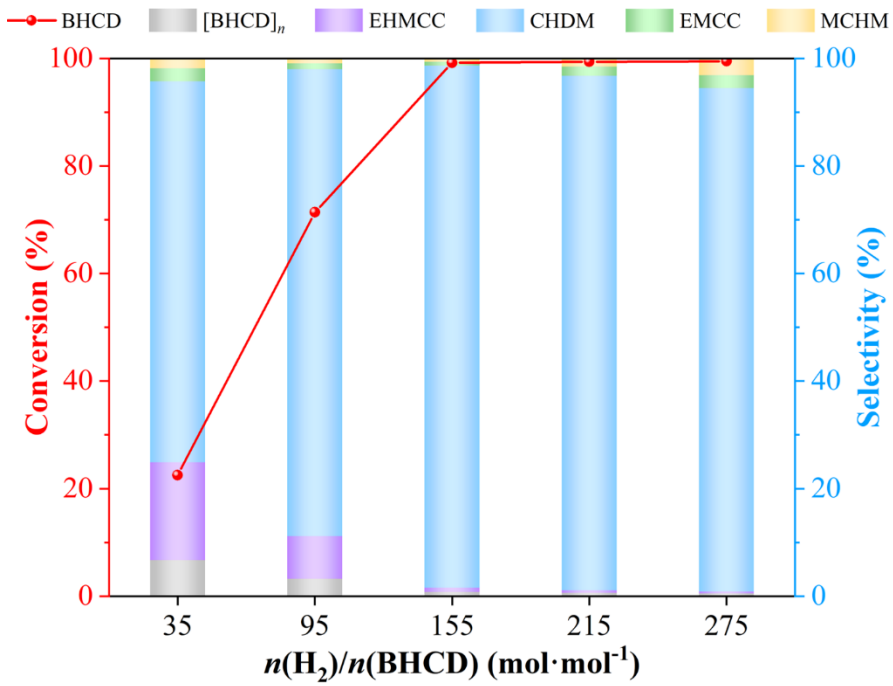

Fig. S13. Performance of Cu/MgO@SiO_2 under varied $n(H_2)/n(BHCD)$.

Reaction conditions: 1 g cat., ω=20wt%, 260 °C, 2.5 MPa H_2, WHSV=0.8 h^{-1}.

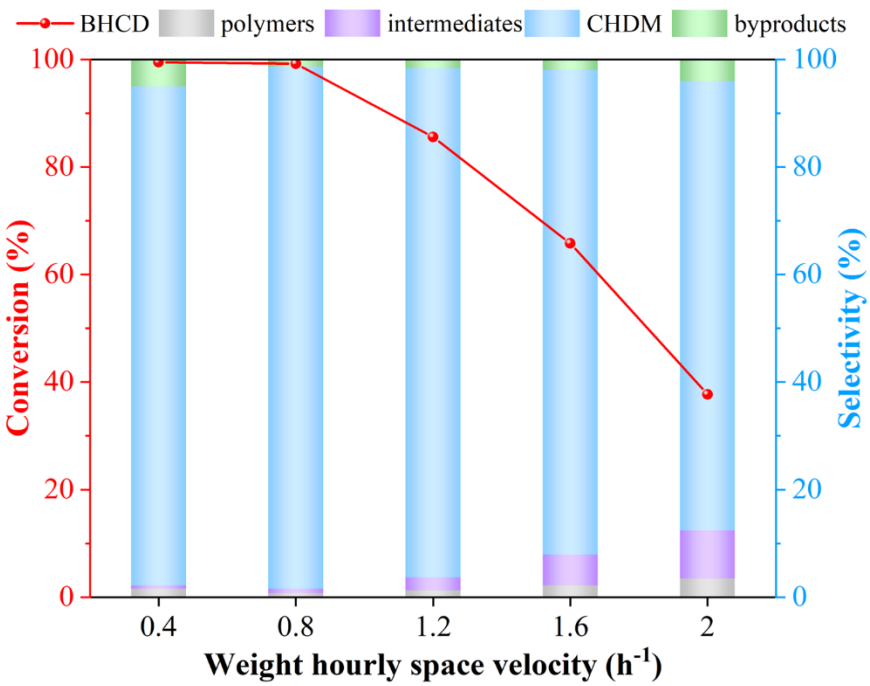

Fig. S14. Performance of Cu/MgO@SiO_2 under varied WHSVs.

Reaction conditions: 1 g cat., ω=20wt%, 260 °C, 2.5 MPa H_2, $n(H_2)/n(BHCD)$=155 mol·mol^{-1}.

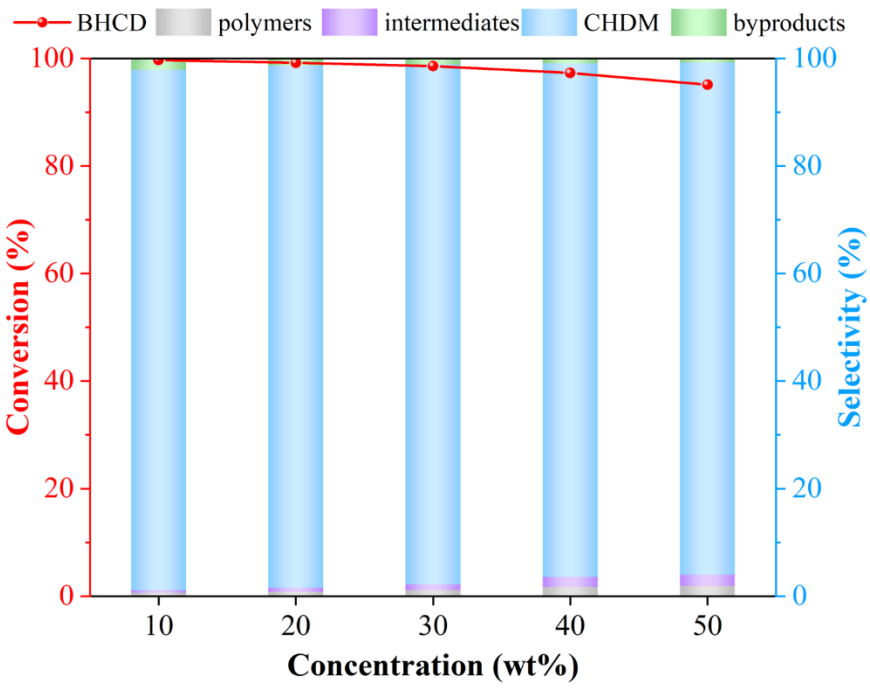

Fig. S15. Performance of Cu/MgO@SiO_2 under varied concentrations in feed.

Reaction conditions: 1 g cat., 260 °C, 2.5 MPa H_2, WHSV=0.8 h^{-1}, $n(H_2)/n(BHCD)$=155 mol·mol^{-1}.

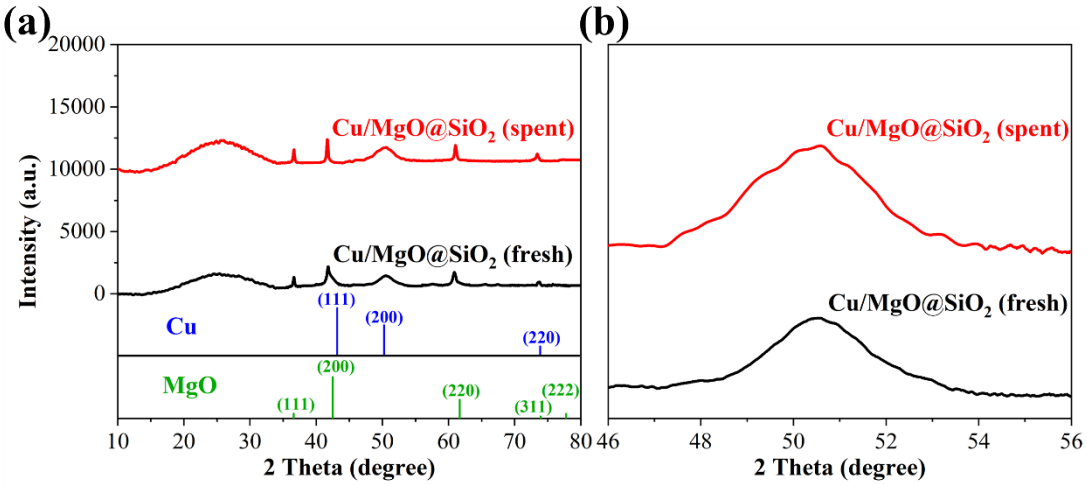

Fig. S16. XRD patterns (a) and enlarged diffraction at 46–56° (b) of fresh and spent $Cu/MgO@SiO_2$.

Table S8. The properties of fresh and spent $Cu/MgO@SiO_2$.

Catalyst	Cu size [a] (nm)	Cu Content (%)	
		Bulk [b]	Surface [c]
$Cu/MgO@SiO_2$ (fresh)	4.6	36.8	14.3
$Cu/MgO@SiO_2$ (spent)	5.5	35.2	13.5

[a] Calculated using Debye-Scherrer Formula from the result of XRD.

[b] Determined using ICP-AES.

[c] Calculated by analyzing XPS.

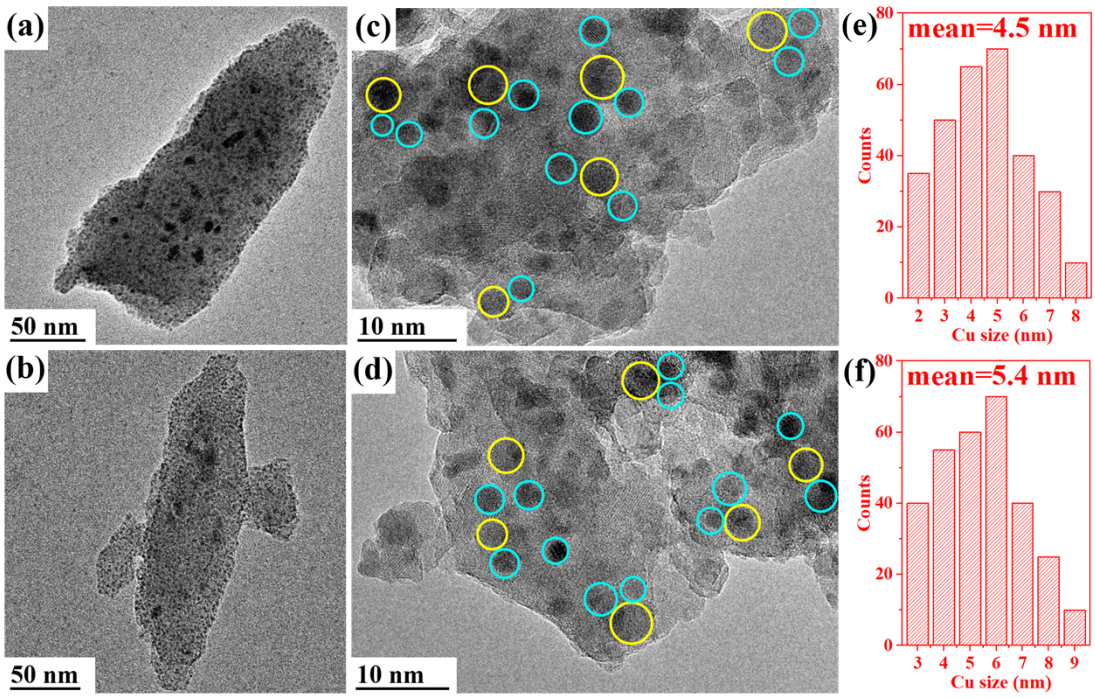

Fig. S17. TEM images and distributions of Cu NPs in fresh (a, c, e) and spent (b, d, f) Cu/MgO@SiO_2.

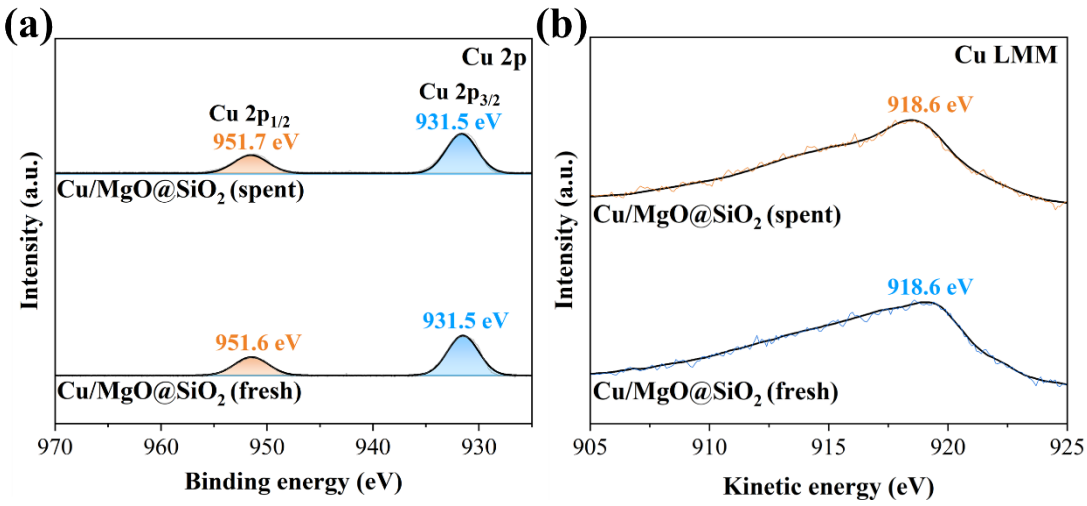

Fig. S18. Binding energy of Cu 2*p* (a) and kinetic energy of Cu LMM (b) in fresh and spent Cu/MgO@SiO_2.

References

1 S. Zhang, Q. Hu, G. Fan and F. Li, *Catal. Commun.*, 2013, **39**, 96–101.

2 S. Zhang, G. Fan and F. Li, *Green Chem.*, 2013, **15**, 2389–2393.

3 Q. Hu, G. Fan, S. Zhang, L. Yang and F. Li, *J. Mol. Catal. A Chem.*, 2015, **397**, 134–141.

4 H. Liu, Q. Hu, G. Fan, L. Yang and F. Li, *Catal. Sci. Technol.*, 2015, **5**, 3960–3969.

5 X. Gong, M. Wang, H. Fang, X. Qian, L. Ye, X. Duan and Y. Yuan, *Chem. Commun.*, 2017, **53**, 6933–6936.

6 Q. Hu, G. Fan, L. Yang and F. Li, *ChemCatChem*, 2014, **6**, 3501–3510.

7 X. Zhou, W. Shen and Y. Fang, *Int. J. Chem. Kinet.*, 2023, **55**, 455–466.

8 Z. Chang, B. Ye, Z. Zhong, S. Wang, H. Wang, W. Du and Z. Hou, *J. Mater. Chem. A*, 2024, **12**, 1003–1011.

9 X. Jiang, Z. Chang, L. Yang, W. Du and Z. Hou, *Fuel*, 2024, **363**, 130944.